Ceramics International 48 (2022) 31344–31353

Contents lists available at ScienceDirect

Ceramics International

journal homepage: www.elsevier.com/locate/ceramint

# $BiLaWO_6$: $Er^{3+}/Tm^{3+}/Yb^{3+}$ phosphor: Study of multiple fluorescence intensity ratiometric thermometry at cryogenic temperatures

K. Pavani [a], A.J. Neves [a,b], Ricardo J.B. Pinto [b], Carmen S.R. Freire [b], M.J. Soares [a], M.P.F. Graça [a], K. Upendra Kumar [c], S.K. Jakka [a,*]

[a] I3N & Department of Physics, University of Aveiro, Aveiro, Portugal
[b] CICECO – Aveiro Institute of Materials, Department of Chemistry, University of Aveiro, 3810-193, Aveiro, Portugal
[c] Department of Physics, School of Applied Sciences, REVA University, Bengaluru, 560064, Karnataka, India

ARTICLE INFO

*Keywords:*
Multicolour upconversion
Cryogenic temperature sensor
Fluorescence intensity ratio
Aurivillius perovskite

ABSTRACT

Highly thermally stable $Er^{3+}/Tm^{3+}/Yb^{3+}$ tri-doped bismuth lanthanum tungstate phosphors were prepared by high temperature solid-state reaction method. The structural and morphological properties of the prepared phosphors were analysed by X-ray diffraction (XRD), Raman spectroscopy and Scanning electron microscopy (SEM) coupled with energy dispersion spectrum (EDS). Visible upconversion (UC) luminescence was measured by exciting the phosphors with 980 nm laser radiation. The dependence of the UC intensity of each emission band of $Er^{3+}$ and $Tm^{3+}$ ions as a function of temperature in the range from 30 to 300 K was monitored. Fluorescence intensity ratios (FIR) of thermally coupled levels (TCL) and non-thermally coupled levels (NTCL) were analysed and verified with appropriate theoretical validation. The absolute ($S_A$) and relative sensitivities ($S_R$) were estimated and compared with the reported systems. In the present case of $BiLaWO_6$: $Er^{3+}/Tm^{3+}/Yb^{3+}$, $S_R$ (0.43 % $K^{-1}$) related to TCL of $Er^{3+}$ UC is found to have maximum sensitivity compared to any of the NTCL combinations at 300 K. From this study we inferred that the $S_R$ values estimated from NTCL are smaller than that of TCL involved in BLW: $Er^{3+}/Tm^{3+}/Yb^{3+}$ phosphor. The temperature dependent CIE color coordinates were also evaluated in the cryogenic temperature region.

## 1. Introduction

Luminescence based thermal sensing is one such kind of technique with modern light-based application apart from the well known direct display applications such as phosphors, scintillators, photocatalysishttps://pubs.rsc.org/en/content/articlehtml/2021/tc/d1tc03202j - cit7 and others [1–5]. Luminescence based thermometry has enormous potential in in vitro and in vivo bio-imaging, medical treatment, in the fields of temperature distribution and maintenance of vast surface areas, electronics, aviation, space research, etc [6–8].

The requirements for optimized luminescent thermometers are due to their thermal sensitivity in the range of temperatures to be examined besides their accuracy, repeatability and stability of the material in the ambiance of measurement. Depending on the measurement conditions, the range of operating temperature is defined. Hence, few phosphors with good sensitivities are not enough for the entire ranges and applications due to diverse environmental conditions. A wide range of phosphors with varied physical, chemical, and even mechanical properties with excellent sensitivities in the desired temperatures ranges are the urgent need.

Aurivillius perovskite family with a general formula $A_{n-1}B_nO_{3n+1}$ (A-12-coordinted and B-6-co-ordinated cations) are well known for their applications in photocatalysis, ferroelectric random-access memories and photoluminescent applications [9,10]. Staking of alternative perovskite and fluorite-like layer favours inducing inherent electric field, which helps in electron-hole pair separation. These kind of compounds exhibit temperature-induced unusual reversible phase transformation and in this case from RT-orthorhombic phase to HT-monoclinic phase. The simplest member is $Bi_2WO_6$, hybridization of Bi 6s and O 2p states in valence band that play a crucial role in shifting of absorption edge towards the visible region. In addition, rare earth (RE) substitution in Bi cationic sites results in the different distribution in conduction band, thus making polymorphs interesting.

Energy level abundancy in $RE^{3+}$ ions leads to emanate excellent luminescence in a vast region from ultraviolet to visible to near infrared regions. Temperature sensing can be done in many ways using

* Corresponding author.,
*E-mail addresses:* suresh@ua.pt, jskphysics@yahoo.co.in (S.K. Jakka).

https://doi.org/10.1016/j.ceramint.2022.06.316
Received 25 March 2022; Received in revised form 15 June 2022; Accepted 29 June 2022
Available online 4 July 2022

luminescence. Basically, divided into three main mechanisms such as (i) spectral (that rely on emission/absorption/excitation line shifts or line widths), (ii) spectral intensity (that rely on the intensity of emission or ratio of emission lines/peaks) and (iii) temporal (that rely on decay/rise time analysis) [11]. The spectral methods require high-resolution instruments while the temporal methods consume too much time for the sensing of accurate temperature. Hence, the mechanism that is feasibly adapted for a wide range of applications could be the spectral intensity method where the ratio of emission lines/peaks is monitored cautiously and systematically. The spectral intensity method which is commonly known as luminescence intensity ratio (LIR) or fluorescence intensity ratio (FIR) technique could be approached in different ways. The most common FIR techniques which uses thermally coupled levels (TCL), where two levels considered to be thermally coupled when they have an energy difference between 200 and 2000 $cm^{-1}$ [12,13]. Dependence of Boltzmann's distribution of energy levels in the excited states is the key working principle in this technique [14]. Next is the ratio of non-thermally coupled levels (NTCL) technique that considers two levels, which are thermally not coupled. Any two emission peaks of active ion/ions whose initial emitting levels' energy difference is more than 2000 $cm^{-1}$ could be used in this technique [15]. One of the other techniques is Valley to Peak ratio (VPR) where the ratio of emission band's peak height and valley between the band with its adjacent could be monitored [16]. Optical thermal sensitivity in the visible region find potential applications in the safety markers. Moreover, sensors at cryogenic temperatures lack high sensitivity, which limits the application in energy and cryogenic research [17]. Tri-doped phosphors with selective lanthanide doping are widely studied owing to their colour tunability upon excitation under different wavelengths, pump power and temperatures [18–21 and references there in].

Taking the advantages of Aurivillius perovskite family and visible (blue, green and red) luminescence of $Er^{3+}$ and $Tm^{3+}$ and FIR, in this work, we have synthesized $Ln^{3+}$ co-doped and tridoped $BiLaWO_6$ phosphor by solid-state reaction method and demonstrated diverse fluorescence intensity ratiometric thermometers based on $Er^{3+}$ and $Tm^{3+}$ ions using TCL and NTCL at cryogenic temperatures in the range 30–300 K upon 980 nm excitation.

## 2. Experimental details

For the preparation of pure and $RE^{3+}$ doped $BiLaWO_6$ phosphor material, a high-temperature solid-state reaction method has been adopted. Stoichiometric amounts of $Bi_2O_3$, $La_2O_3$, $WO_3$, $Ln_2O_3$ oxides (Ln = $La^{3+}$, $Er^{3+}$, $Tm^{3+}$ and $Yb^{3+}$) were purchased and taken in an agate mortar, mixed thoroughly in acetone for homogenous grinding and sintered at 1000 °C for 3 h. $BiLa_{(1-x-y-z)}WO_6$: x $Er^{3+}$-y $Tm^{3+}$- z $Yb^{3+}$, (where x = 1.0, y = 2.0 and z = 10, in mol%) is abbreviated as BLW: Er/Tm/Yb and the same composition characterised for FIR based on TCL and NTCL at cryogenic temperatures.

Phase purity and crystal structure were characterized by the X-ray diffraction method with Philips Analytical X'pert Pro analyzer equipped with Cu-Kα radiation (λ = 1.54178 Å). The morphology of prepared powders was investigated by carbon coating using a scanning electron microscope (SEM) (TESCAN VEGA3 instrument) equipped with Energy Dispersive X-ray analysis (EDS). Raman spectrum was collected on Horiba HR 800 spectrometer in reflection geometry mode by exciting the sample with blue (442 nm) laser and using 50× magnification with a resolution of at least 7 $cm^{-1}$. The Fourier transform infrared-attenuated total reflection (FTIR-ATR) spectra were collected in a BX spectrometer (PerkinElmer, Waltham, MA, USA), coupled with a single horizontal Golden gate ATR cell (Specac®, London, UK), using 64 scans at a resolution of 4 $cm^{-1}$. Optical absorption and diffuse reflectance spectra were measured using Jasco V-560 spectrophotometer coupled with an integrating sphere, within the wavelength region 250–850 nm.

High-resolution UC luminescence spectra with varying temperatures were recorded using a Spex 1704 monochromator coupled with a Hamamatsu R928 photomultiplier tube with a resolution of ~0.01 nm by exciting the samples with an NIR (980 nm) laser. PL was measured at temperatures between 30 and 300 K sensed with thermocouple of ± 2 K error using a closed-cycle helium cryostat consisting of APD Cryogenic closed-cycle helium system having two-stage cryogenic refrigerator DE-204SL with water-cooled helium compressor, based on the Gifford–McMahon cycle.

## 3. Results and discussion

### 3.1. Structural and morphological studies

The phase identification of prepared undoped and tri-doped BLW phosphors' was evaluated by XRD technique and the pattern are shown in Fig. 1(a). All diffraction peaks were well in accordance with the standard ICDD: 00-033-0203 pattern and possessed a monoclinic phase with the space group P2/a. Doping of rare-earths ($Er^{3+}$/$Tm^{3+}$/$Yb^{3+}$) in place of $La^{3+}$ induced shift of diffraction peaks towards higher 2θ angles as shown in the inset of Fig. 1(a). Based on Bragg's equation $2d\sin\theta = n\lambda$, when the ions of smaller ionic radii, ($Er^{3+}$, $Tm^{3+}$ and $Yb^{3+}$) occupy the position of larger ionic radius ($La^{3+}$) ion in the matrix, the crystal plane spacing decreases and hence the diffraction peaks shift towards larger angle. The crystallite size ($D$) was calculated using Debye-Scherrer equation:

$$D = \frac{k\lambda}{\beta \cos\theta} \quad (1)$$

where $\beta$ is the full width at half maximum of the pure diffraction profile in radians, $k$ is a constant (0.9), θ is the diffraction angle. The estimated average crystallite size is in the range of 60–85 nm. The calculated lattice parameters and unit cell volume are (monoclinic phase α = γ = 90°): a = 16.484 Å, b = 7.712 Å, c = 8.249 Å, β = 101.91, V = 1025.99 × $10^{-30}$ $m^3$ and a = 16.397 Å, b = 7.682 Å, c = 8.239 Å, β = 101.94, V = 1015.44 × $10^{-30}$ $m^3$ for BLW and BLW:Er/Yb/Tm, respectively.

Fig. 1 (b & c) illustrate the well-resolved normalized Raman and FTIR- ATR spectra of undoped and tri-doped BLW phosphors. High energy phonon peak was found to be around 897 $cm^{-1}$, which is the characteristic nature of the asymmetric stretching vibrational mode of $WO_6$ (Apical O). From previous observations, it has been concluded that the position of this peak is RE sensitive. The peak position is associated with the ionic radius of $RE^{3+}$ taking the position of $Bi^{3+}$ in $Bi_2WO_6$ [22,23]. Other intense peaks in the region 600-800 $cm^{-1}$ are associated with symmetric stretching and asymmetric stretching vibrations of $WO_6$ (Apical O) and $WO_6$ (Equatorial O) bands [23]. Relative intensities of these two bands are observed as Er/Tm/Yb occupies La position in the BLW matrix. The bands in between 200 and 600 $cm^{-1}$ were originated from bending modes of $WO_6$ octahedra and coupled with bending, stretching bands of bismuth-oxygen polyhedra. In this region, no additional changes were observed upon doping.

As observed in Fig. 1 (c), the FTIR-ATR spectra consist of several bands within 1000 and 400 $cm^{-1}$. Overlapped high intense bands centered at 655 and 734 $cm^{-1}$ are ascribed to W–O–W bending modes and stretching modes are in the region 850-950 $cm^{-1}$ [24–26]. The remaining bands in 400–550 $cm^{-1}$ lower wavenumber region are the resultant of (Bi, La)–O bending modes of $BiO_6$.

Diffuse reflectance spectra (DRS) of undoped and tri-doped BLW phosphors are shown in Fig. 1 (d). In both the cases broadband in the lower wavelength region (200–475 nm) is originated as a result of La–O charge transfer band (CTB), $Bi^{3+}$ ($^1S_0 \rightarrow {}^3P_1$) and ligand to metal charge transfer transition (LMCT) of W–O. While $Er^{3+}$ ($^4I_{15/2} \rightarrow {}^2H_{11/2}$, $^4I_{15/2} \rightarrow {}^4F_{9/2}$, $^4I_{15/2} \rightarrow {}^4I_{9/2}$) and $Tm^{3+}$ ($^3H_6 \rightarrow {}^3F_{2,3}$ & $^3H_6 \rightarrow {}^3F_4$) sharp absorption transitions are observed in visible and IR regions. The absorption edge is shifted towards a higher wavelength region when the BLW matrix is doped with $Ln^{3+}$ ions and is associated with dopant and host ionic radii difference and chemical nature of the dopant ions. Corresponding

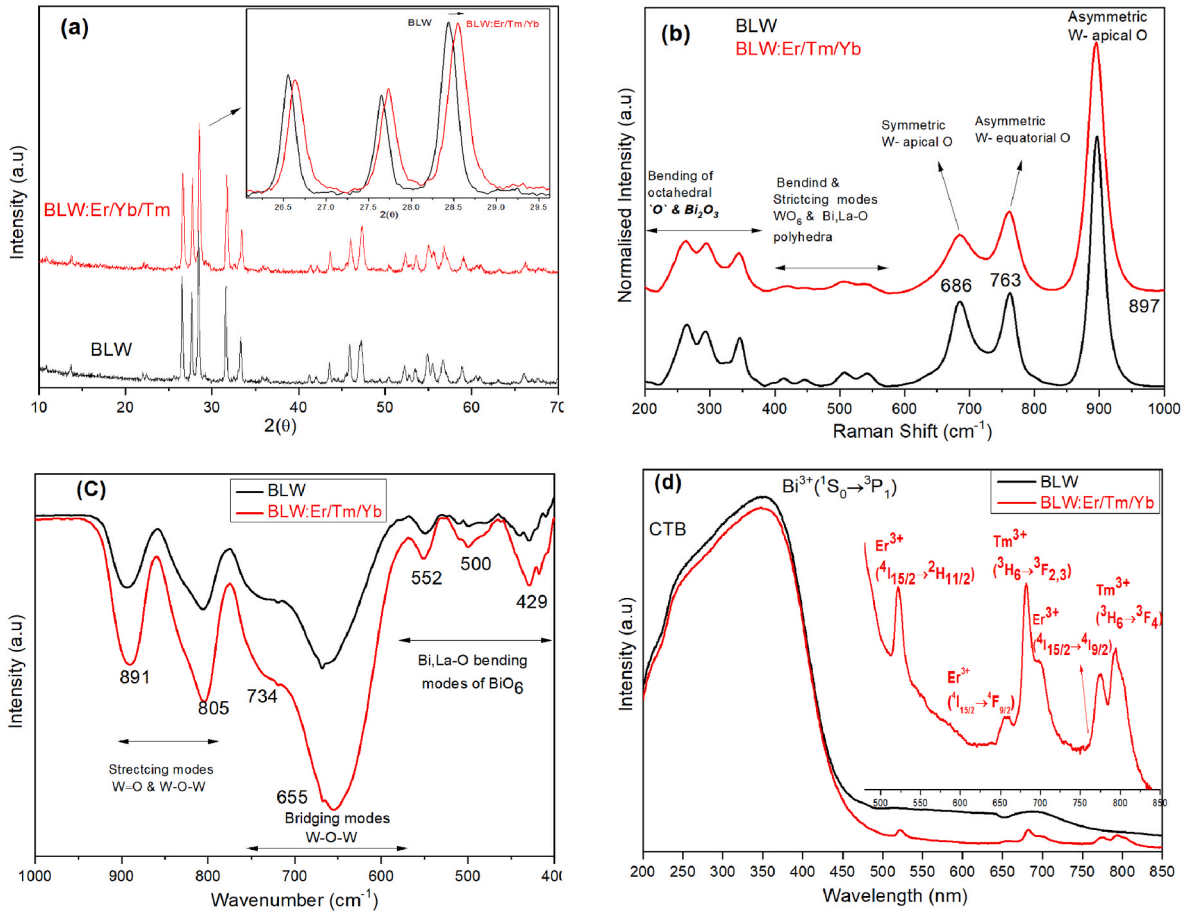


**Fig. 1.** (a)XRD (Inset shows the enlarged XRD portion of high intense peaks), (b) Raman, (c) FTIR-ATR and (d) DRS patterns of BLW & BLE:Er/Tm/Yb phosphors.

bandgap values are calculated using the Tauc and Davis-Mott plot [23, 27] and are in the range of approximately 2.2 eV.

Fig. 2(a) depicts SEM micrograph along with particle size distribution (inset). Particles are found to be spherical in shape while their mean particle size is estimated to be ~500 nm. Energy dispersion spectrum (EDS) and elemental distribution mapping of BLW phosphor are shown in Fig. 2 (b). The constituents of phosphor material are found to be homogeneously distributed throughout the sample without any elemental segregation.

### 3.2. Upconversion photoluminescence

Fig. 3(a) presents the room temperature visible UC-PL of BLW:Er/Yb, BLW:Tm/Yb and BLW:Er/Tm/Yb phosphors by exciting at 980 nm laser radiation. The spectra composed of emission bands in blue, green, red and far-red regions that are the combinations of UC emissions from both $Tm^{3+}$ and $Er^{3+}$ ions. The emission bands centered at 475, and 700 nm were assigned to $^1G_4 \rightarrow {}^3H_6$, and $^3F_3 \rightarrow {}^3H_6$ transitions of the $Tm^{3+}$ ions, respectively. On the other hand, the emission bands centered at 525 and 540 nm (Green) were assigned to $^2H_{11/2}$, $^4S_{3/2} \rightarrow {}^4I_{15/2}$ transitions of $Er^{3+}$. But, the emission band centered around 650 nm (red) is regarded as a combination of two transitions $^4F_{9/2} \rightarrow {}^4I_{15/2}$ and $^1G_4 \rightarrow {}^3F_4$ from

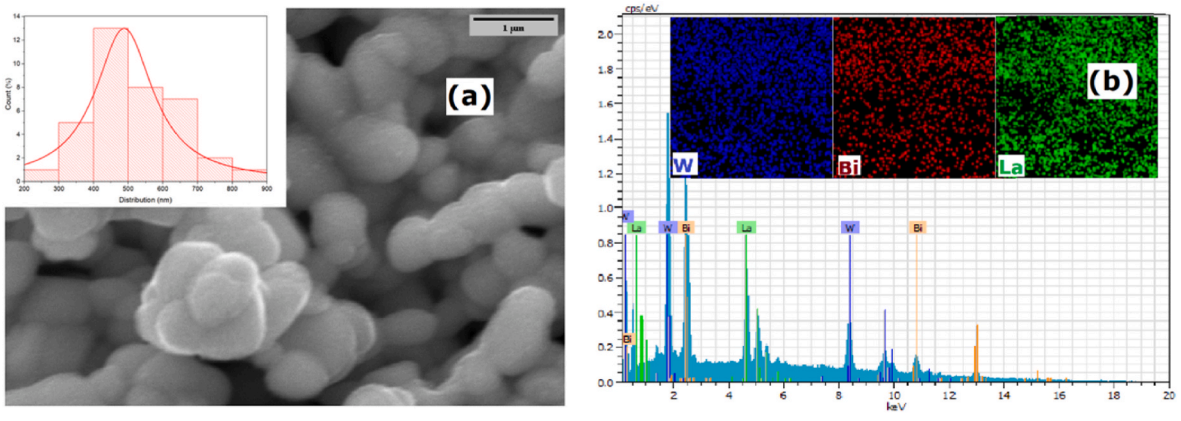


**Fig. 2.** (a) SEM, particle size distribution diagram (inset) (b) EDS and elemental mapping of $W^{6+}$, $La^{3+}$ and $Bi^{3+}$ ions in BGW phosphor.

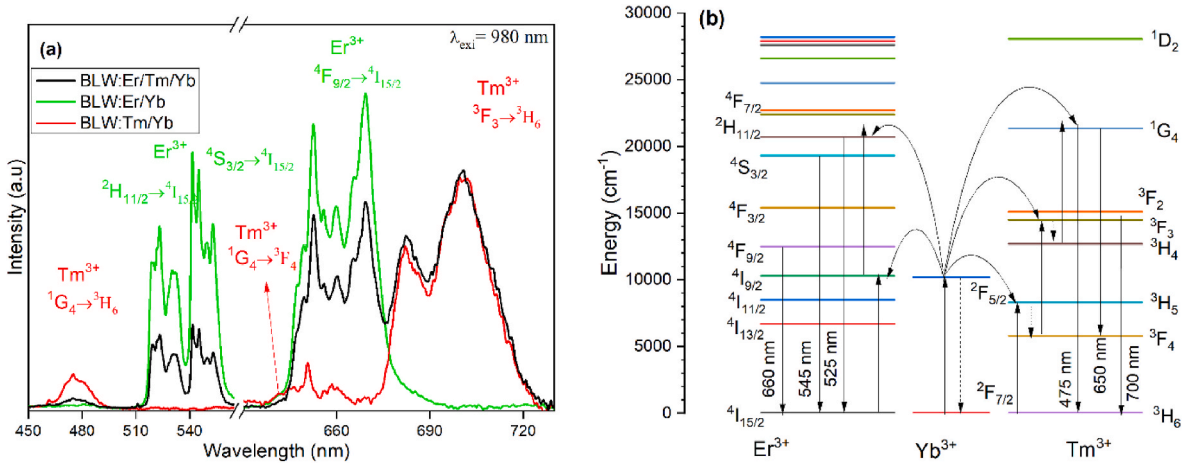


**Fig. 3.** (a) Visible room temperature upconversion and (b) Partial energy level diagram of BLW:Er/Tm/Yb phosphor excited with 980 nm laser radiation (power = 450 mW and spot size about 4 $mm^2$).

$Er^{3+}$ and $Tm^{3+}$ ions which was also observed from the emission spectra of BLW:Er/Yb and BLW:Tm/Yb as shown Fig. 3(a). (Note that the similar procedure has been followed for the preparation of BLW:$Er_{01}$/$Yb_{10}$ and BLW:$Tm_{02}$/$Yb_{10}$ phosphors as that of BLW: Er/Tm/Yb). Further, the splitting of these emission bands are realized from the crystal field effect. Among all dopant ions, while exciting with the NIR (980 nm) laser, $Yb^{3+}$ ion always acts as a sensitizer and transfer the energy to other $RE^{3+}$ ions namely $Er^{3+}$ and $Tm^{3+}$. The energy transfer from $Yb^{3+}$ to $Er^{3+}$/$Tm^{3+}$ and pumping of electrons to the excited states leads to upconversion (visible) emission from the latter ions. Fig. 3(b) depicts the partial energy level diagram presenting the detailed UC mechanisms involved in the tri-doped BLW: Er/Tm/Yb phosphor. The emission of 475 nm and 650 nm from $Tm^{3+}$ evolved by the three photon process. The emission of 540 nm ($Er^{3+}$), 650 nm ($Er^{3+}$) and 700 nm ($Tm^{3+}$) emission is found to be a two photon process. Also noted that the intensity of red emission enhanced than that of the blue/green emission from $Tm^{3+}$/$Er^{3+}$ as the concentration of $Tm^{3+}$ or $Er^{3+}$ or $Yb^{3+}$ are relatively high in BLW. And hence, not only the energy transfer from $Yb^{3+}$ ions to $Er^{3+}$ and $Tm^{3+}$, but also some of the other energy transfers and back transfers among $Er^{3+}$ and $Tm^{3+}$ ions are expected which leads to cross-relaxations and quenching with increase of temperatures or concentrations of the active ions. The mechanism underlying in upconversion process of tri-doped materials was well explored in the literature [28–34].

### 3.3. Temperature dependent upconversion

The UC spectra with change in the sample temperature have been recorded for BLW: Er/Tm/Yb with in the temperature range of 30 and 300 K. The UC spectra were normalized with reference at 700 nm for the sake of convenience and has been presented in Fig. 4(a). Significant changes were observed in the emission intensities of different UC bands from both $Er^{3+}$ and $Tm^{3+}$ ions. None of the emission peaks has a concurrent thermal behaviour with that of the others as it should be understood that all the peaks have a different origin (starting state) either it is of different or of the same activator ion. The changes in the intensity of different peaks in the UC emission spectra of BLW:Er/Tm/Yb has been plotted as a function of temperature and is shown in Fig. 4(b). The dependence of intensity on temperature could be related to the modified Arrhenius equation [35–37].

$$I(T) = \frac{I_0}{1 + A\exp\left(\frac{-E_a}{k_B T}\right)} \quad (2)$$

where $I_0$ is the emission intensity at T = 0 K, $A = \frac{A_{NR}}{A_R}$ = Ratio of non-radiative and radiative transition probabilities, $E_a$ being the activation energy of thermal quenching and $k_B$ is the Boltzmann's constant. All the intensity trends (dots) of the five UC bands have been well fitted (solid line) with Eq. (2) as shown in Fig. 4(b).

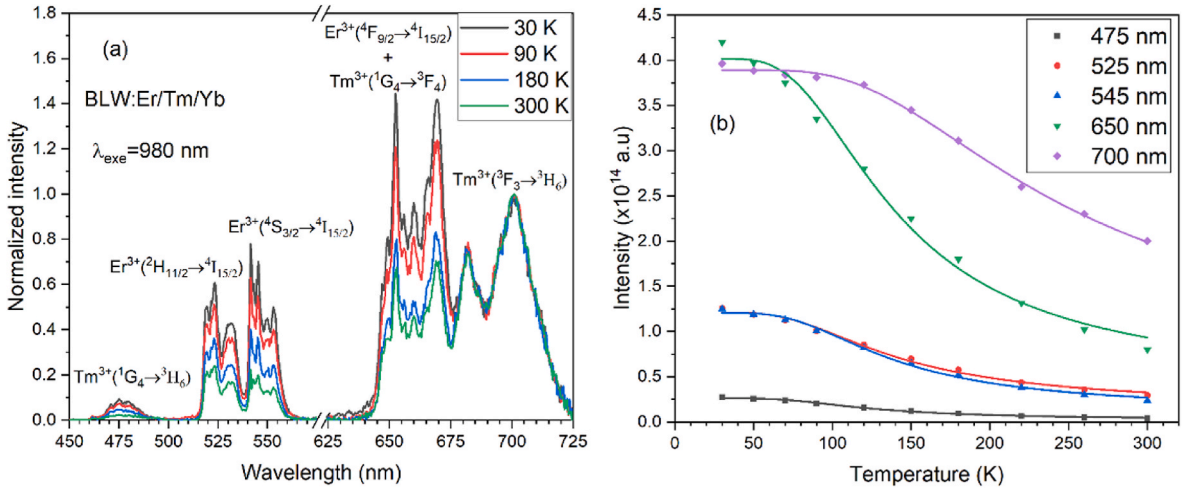


**Fig. 4.** Temperature dependent upconversion (a) spectra in the region 450–730 nm and (b) intensity trends of various peaks in BLW:Er/Tm/Yb phosphor when excited with 980 nm radiation.

### 3.4. Thermal sensitivities

The emission bands as discussed above are represented by the peak central wavelengths namely 475, 525, 545, 650 and 700 nm, for the transitions $^1G_4 \rightarrow {}^3H_6$ ($Tm^{3+}$), $^2H_{11/2} \rightarrow {}^4I_{15/2}$ ($Er^{3+}$), $^4S_{3/2} \rightarrow {}^4I_{15/2}$ ($Er^{3+}$), $^4F_{9/2} \rightarrow {}^4I_{15/2}$ ($Er^{3+}$) + $^1G_4 \rightarrow {}^3F_4$ ($Tm^{3+}$) and $^3F_3 \rightarrow {}^3H_6$ ($Tm^{3+}$), respectively. Fig. 6(a–d) represent different combinations of the FIRs. Fig. 5(a) presents FIR related to TCL of $Er^{3+}$ emission peaks $I_{525}/I_{545}$. Fig. 5(b) and (c) presents FIR related to NTCL of $Er^{3+}$emission peaks $I_{525}/I_{650}$ and $I_{650}/I_{545}$ nm of $Er^{3+}$ and $I_{700}/I_{475}$ nm of $Tm^{3+}$, respectively. Fig. 5(d) presents the Intensity ratio of different NTCL levels each from different activator ($Er^{3+}/Tm^{3+}$) ions.

FIR of TCL pertaining to $Er^{3+}$ ions in BLW:Er/Tm/Yb phosphor could be related to Eq. (3) which is a consequence of Boltzmann's distribution law as the two energy levels $^2H_{11/2}$ and $^4S_{3/2}$ are close to each other and occupation of ions at $^2H_{11/2}$ at any particular temperature will have a portion influenced by population of ions at $^4S_{3/2}$ and hence the ratio could be as follows [13,38–40].

$$FIR(TCL) = \frac{I_{525}}{I_{545}} = A + Bexp\left(\frac{-\Delta E}{k_B T}\right) \tag{3}$$

where $I_{525}$ nm and $I_{550}$ nm are the UC band intensities of the two green emissions, A is a constant, ΔE is the energy gap between the $^2H_{11/2}$ and $^4S_{3/2}$ levels, $K_B$ is the Boltzmann constant, and T is the absolute temperature.

The absolute sensitivity ($S_A$) which is defined as the rate of change in the *FIR* in response to the variation in temperature. Hence the $S_A$ of the TCL can be expressed as

$$S_A(TCL) = \frac{d}{dT}(FIR) = \frac{B\Delta E}{KT^2} exp\left[\frac{-\Delta E}{KT}\right] \tag{4}$$

To allow the comparison of sensitivities of different materials, relative sensitivity has been derived by the following relation

$$S_R(TCL) \cong \frac{1}{FIR}\frac{d}{dT}(FIR) = \frac{\Delta E}{KT^2} \tag{5}$$

In the case of NTCL, FIR cannot be treated with Eq. (3) as the two states involved are not related through the Boltzmann's law. Hence considering the intensity trends of Eq. (2) for the two transitions, the FIR of NTCL can be derived and simplified by the Taylor expansion method, as follows [34,35].

$$FIR(NTCL) = \frac{\frac{I_{01}}{1+A_1\ exp\left(\frac{-\Delta E_1}{k_B T}\right)}}{\frac{I_{02}}{1+A_2\ exp\left(\frac{-\Delta E_2}{k_B T}\right)}} = A + Bexp\left(\frac{-\Delta E'}{k_B T}\right) \tag{6}$$

where A, B and $-\Delta E'$ are constants dependent on $I_{01}$, $I_{02}$, $A_1$, $A_2$, $\Delta E_1$ and $\Delta E_2$. In this case, the sensitivities $S_A$ and $S_R$ thus can be written as

$$S_A(NTCL) = \left|\frac{dFIR}{dT}\right| = B\frac{\Delta E'}{k_B T^2} exp\left(\frac{-\Delta E'}{k_B T}\right) \tag{7}$$

$$S_R(NTCL) = \left|\frac{1}{FIR}\frac{dFIR}{dT}\right| \times 100\% = \frac{B\frac{\Delta E'}{k_B T^2}\exp\left(\frac{-\Delta E'}{k_B T}\right)}{A + Bexp\left(\frac{-\Delta E'}{k_B T}\right)} \tag{8}$$

The FIRs thus calculated and presented in Fig. 5(a–d) are systematically fitted with Eq. (3) for $Er^{3+}$ TCL in Fig. 5 (a) and Eq. (6) for the remaining sets of NTCL of $Er^{3+}$, $Tm^{3+}$ and $Er^{3+}/Tm^{3+}$ combinations as shown in Fig. 5(b–d), respectively. It is to be noted that Eq. (6) considers the energy transfer and back transfer among the activator ions which also affects the sensitivities. Table 1 presents the complete fitting parameters related to the FIR of TCL and NTCL fittings using Eqs. (3) and (6). It could be noted that the FIR of NTCL pertaining to the peaks 650 nm and 545 nm presented in Fig. 5 (b) could not be fit with Eq. (6). This may be due to the involvement of $Er^{3+}$ ($^4F_{9/2} \rightarrow {}^4I_{15/2}$) and $Tm^{3+}$ ($^1G_4 \rightarrow$

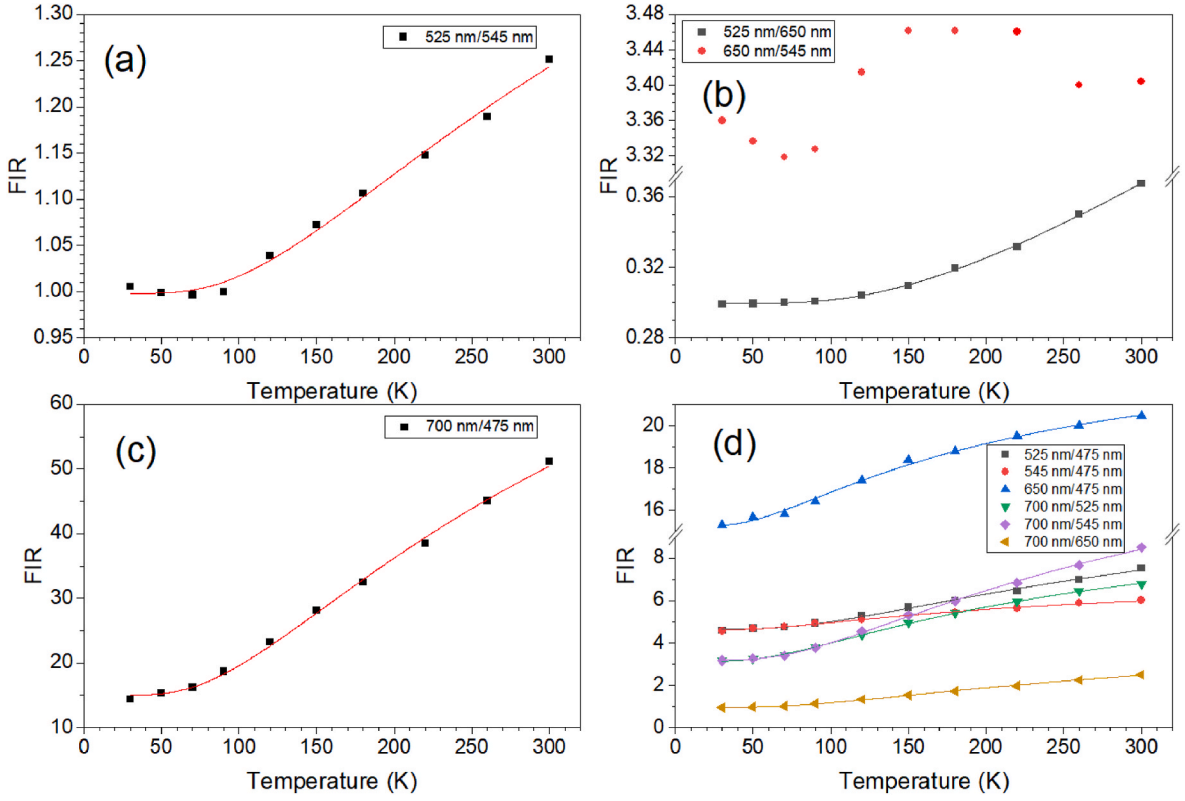


**Fig. 5.** Fluorescence intensity ratios of (a) TCL of $Er^{3+}$, (b) NTCL of $Er^{3+}$, (c) NTCL of $Tm^{3+}$and (d) NTCL of $Er^{3+}/Tm^{3+}$ ions in BLW:Er/Tm/Yb phosphor upconversion emission bands at different temperatures.

**Table 1**
Fitting parameters A, B and ΔE/ΔE′ of different FIRs pertaining to different combinations of transitions

| FIR type | FIR Ratio combination in nm | A | B | ΔE/ΔE′ |
|---|---|---|---|---|
| TCL (Er) | 525/545 | 0.998 | 0.885 | 267.19 |
| NTCL (Er1) | 525/650 | 0.299 | 0.464 | 402.56 |
| NTCL (Tm) | 700/475 | 15.029 | 98.651 | 213.59 |
| NTCL (Er/Tm)-1 | 525/475 | 4.657 | 7.880 | 217.09 |
| NTCL (Er/Tm)-2 | 545/475 | 4.612 | 2.714 | 142.59 |
| NTCL (Er/Tm)-3 | 650/475 | 15.263 | 9.499 | 124.16 |
| NTCL (Er/Tm)-4 | 700/525 | 3.135 | 7.644 | 151.95 |
| NTCL (Er/Tm)-5 | 700/545 | 3.189 | 13.259 | 193.84 |
| NTCL (Er/Tm)-6 | 700/650 | 0.967 | 4.052 | 206.56 |

$^3F_4$) UC transitions which have more complicated order of intensity compared to the other transitions.

Based on the fitting parameters and using Eqs. (4) and (5) for TCL and Eqs. (7) and (8) for NTCL, $S_A$ and $S_R$ have been calculated and presented in Fig. 6 (a and b) for the FIR related to TCL and Fig. 6(c and d) for the FIRs related to NTCL in this study. It is noted that the $S_A$ values of all the FIRs (Fig. 6(a and c)) increases to a certain temperature and decreases gradually. The maximum values of $S_A$ of all the FIRs tend to be between 100 K and 150 K. Among all the $S_A$ values, the FIR($I_{545}/I_{700}$) has the highest value of 0.17 $K^{-1}$ at 140 K.

Regarding the $S_R$ values, the trends of $S_R$ of NTCL (Fit. 6(d)) were also observed to be similar to that of $S_A$ (Fig. 6(c)). The $S_R$ was increased till a certain threshold temperature and then decreased. The $S_R$ values were found to be maximum below 100 K for all the NTCL FIRs. Whereas the $S_R$ of TCL (Fig. 6(b)) is found to be exponentially decreasing and it has the maximum compared to all the NTCL combinations also. Though NTCL has been expected to have $S_R$ values greater than TCL, that phenomenon has not been realized in the present case due to the energy transfer between the two activator ions ($Er^{3+}$ and $Tm^{3+}$) and the back transfer as predicted elsewhere [34].

Table 2 presents the FIRs drawn from TCL and NTCL of different matrices doped with selective Lanthanide ions, transitions involved therein and also the respective $S_R$ at 300 K. The $S_R$ values estimated from NTCL are smaller than that of TCL involved in BLW: Er/Tm/Yb phosphor and maybe due to the energy transfers or complications in the estimation of the energy transfer mechanisms in the material thus quenching the luminescence or UC behaviour and sensing less effectively. The present studied BLW: Er/Tm/Yb with two activator ions and a sensitizer ion has also shown a better sensitivity at room temperature than the reported tri-doped materials with TCL with emission lines in visible range [41, 42].

While Table 2 presents the $S_R$ values of different UC materials at 300 K based on FIR, Table 3 presents a comprehensive comparison of both the TCL and NTCL sensitivities of different materials in the cryogenic temperature ranges [15,45–56]. There were very few reports on the cryogenic temperature ranges due to the complexity of the experimental design. But the applications of this kind of optical sensors are very essential with increasing sensor applications in these temperature regions. The emitting centres in Table 3 are not limited to the emission centres of the present work, rather they are compared with the most recent literature at low temperatures with emission in the visible region. Sensitivities of FIR based on TCL and NTCL are compared independently. Regarding FIR based on TCL, in the present work, the maximum values of $S_A$ and $S_R$ are achieved at 30 K and 190 K, respectively. The sensitivities in different works widely depend on the characteristics of the host, selection of dopants and the range of temperature. Streamlining different host materials for comparison is of utmost importance. In Table 3, it could be observed that different materials have maximum sensitivities at different temperatures. For example, $YbNbO_4:Er^{3+}$ has maximum $S_a$ at 220 K, $Na_{0.5}Bi_{0.5}TiO_3:Ho^{3+}/Yb^{3+}$ has maximum $S_A$ and $S_R$, both at 167 K and $TeO_2$-$PbCl_2$-$WO_3$:$Er^{3+}$ glass has a maximum $S_A$ at 100 K. Also, the trend of each $S_A$ and $S_R$ curve depends on the respective host-dopant combinations. While comparing with different materials,

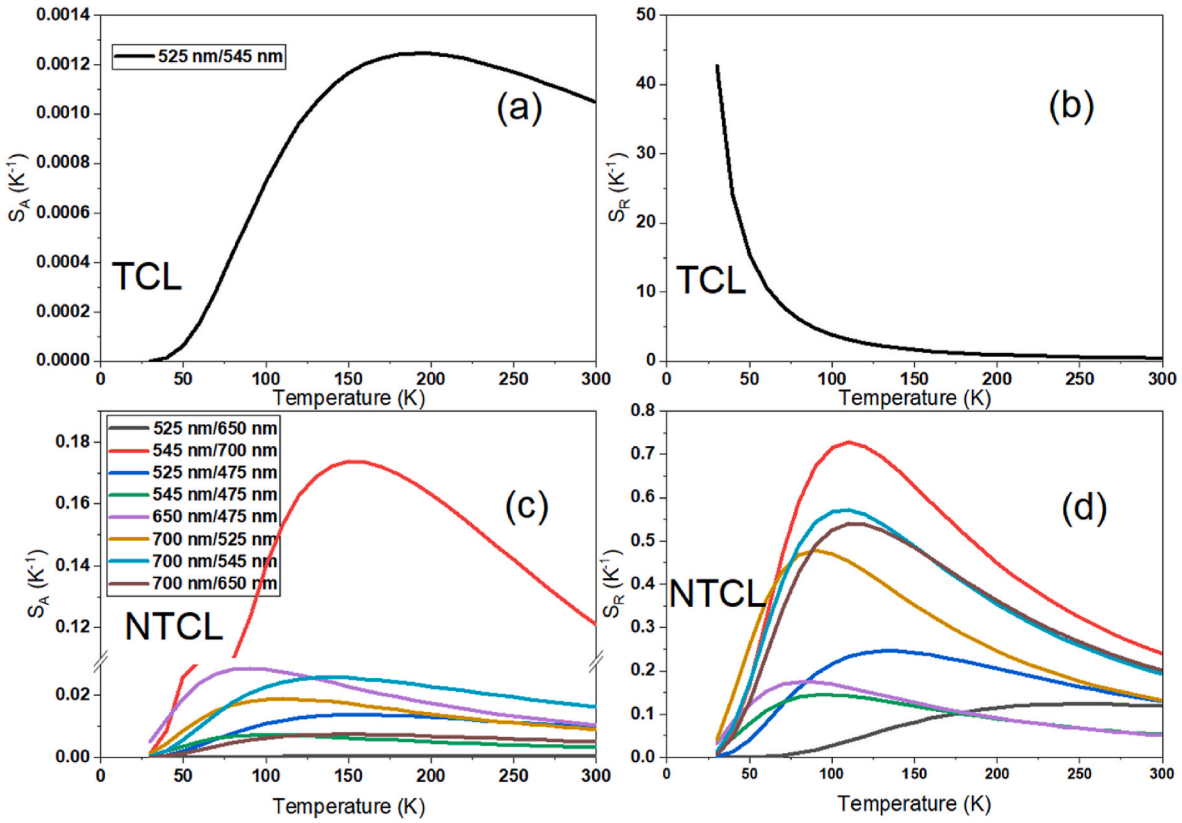


**Fig. 6.** Absolute ($S_A$) and relative ($S_R$) sensitivities of (a,b) TCL and (c,d) NTCL FIRs of BLW:Er/Tm/Yb phosphor excited at 980 nm as a function of temperature.

**Table 2**
Relative sensitivities ($S_R$ % $K^{-1}$) of different compositions at 300 K.

| Host | Ions | Transitions | Ratio, λ (nm) | $S_R$ (% $K^{-1}$) | Reference |
|---|---|---|---|---|---|
| BLW | $Er^{3+}$/ $Tm^{3+}$/ $Yb^{3+}$ | $^2H_{11/2} \rightarrow {}^4I_{15/2}$ ($Er^{3+}$)/$^4S_{3/2} \rightarrow {}^4I_{15/2}$ ($Er^{3+}$) | 525/ 545 | 0.43 | This work |
| | | $^2H_{11/2} \rightarrow {}^4I_{15/2}$ ($Er^{3+}$)/($^4F_{9/2} \rightarrow {}^4I_{15/2}$ ($Er^{3+}$) + $^1G_4 \rightarrow {}^3F_4$ ($Tm^{3+}$)) | 525/ 650 | 0.19 | |
| | | $^3F_3 \rightarrow {}^3H_6$ ($Tm^{3+}$)/$^1G_4 \rightarrow {}^3H_6$ ($Tm^{3+}$) | 700/ 475 | 0.24 | |
| | | $^2H_{11/2} \rightarrow {}^4I_{15/2}$ ($Er^{3+}$)/$^1G_4 \rightarrow {}^3H_6$ ($Tm^{3+}$) | 525/ 475 | 0.13 | |
| | | $^4S_{3/2} \rightarrow {}^4I_{15/2}$ ($Er^{3+}$)/$^1G_4 \rightarrow {}^3H_6$ ($Tm^{3+}$) | 545/ 475 | 0.05 | |
| | | ($^4F_{9/2} \rightarrow {}^4I_{15/2}$ ($Er^{3+}$) + $^1G_4 \rightarrow {}^3F_4$ ($Tm^{3+}$))/$^1G_4 \rightarrow {}^3H_6$ ($Tm^{3+}$) | 650/ 475 | 0.05 | |
| | | $^3F_3 \rightarrow {}^3H_6$ ($Tm^{3+}$)/$^2H_{11/2} \rightarrow {}^4I_{15/2}$ ($Er^{3+}$) | 700/ 525 | 0.13 | |
| | | $^3F_3 \rightarrow {}^3H_6$ ($Tm^{3+}$)/$^4S_{3/2} \rightarrow {}^4I_{15/2}$ ($Er^{3+}$) | 700/ 545 | 0.19 | |
| | | $^3F_3 \rightarrow {}^3H_6$ ($Tm^{3+}$)/ ($^4F_{9/2} \rightarrow {}^4I_{15/2}$ ($Er^{3+}$) + $^1G_4 \rightarrow {}^3F_4$ ($Tm^{3+}$)) | 700/ 650 | 0.20 | |
| $Ba_3Y_4O_9$ | $Er^{3+}$/ $Tm^{3+}$/ $Yb^{3+}$ | $^2H_{11/2} \rightarrow {}^4I_{15/2}$ ($Er^{3+}$)/$^1G_4 \rightarrow {}^3H_6$ ($Tm^{3+}$) | 537/ 482 | 0.78 | [19] |
| $Ba_3Y_4O_9$ | $Er^{3+}$/ $Tm^{3+}$/ $Yb^{3+}$ | $^1G_4 \rightarrow {}^3H_6$ ($Tm^{3+}$)/$^4S_{3/2} \rightarrow {}^4I_{15/2}$ ($Er^{3+}$) | 482/ 560 | 0.21 | [19] |
| $Y_2O_3$ | $Ho^{3+}$/ $Tm^{3+}$/ $Yb^{3+}$ | $^1G_4 \rightarrow {}^3H_6$ ($Tm^{3+}$)/$^5F_3 \rightarrow {}^5I_8$ ($Ho^{3+}$) | 541/ 490 | 0.01 | [41] |
| $Bi_{1.81}MoO_6$ | $Er^{3+}$/ $Tm^{3+}$/ $Yb^{3+}$ | $^3F_{2,3} \rightarrow {}^3H_6$ ($Tm^{3+}$) $^2H_{11/2} \rightarrow {}^4I_{15/2}$ ($Er^{3+}$) | 700/ 525 | 5.59 | [42] |
| β′$Gd_2(MoO_4)_3$ | $Er^{3+}$/ $Tm^{3+}$/ $Yb^{3+}$ | $^3F_2 \rightarrow {}^3H_6$ ($Tm^{3+}$)/$^3H_4 \rightarrow {}^3H_6$ ($Tm^{3+}$) | 700/ 800 | 3.3 | [43] |
| CaWO4 | Er3+/ Yb3+/ Li+/ Nb5+ | 2H11/2(Er3+)/4S3/ 2(Er3+) | 531/ 553 | 1.34 | [44] |

the present material BLW: Er/Tm/Yb has a better $S_A$ and $S_R$ at its maximum points.

While coming to the FIR based on NTCL, there exist different mathematical interpretations researchers use to interpret the FIR of different emission bands of the same spectrum. Hence the $S_A$ and $S_R$ could be entirely of different trends and sometimes could have constant values in the entire temperature range [15,45–56] in the studies depending on the mathematical interpretation. However, in the present work, BLW:Er/Tm/Yb achieved maximum $S_A$ and $S_R$ at 150 and 110 K, respectively. Overall, the BLW:Er/Tm/Yb has interesting sensitivities in the visible region at the cryogenic temperatures compared to other reported systems in the literature.

Repeatability is one of the important aspects to be considered while choosing sensing materials. Fig. 7 depicts the plot of FIR of BLW:Er/Tm/Yb phosphor with the heating and cooling the sample for a couple of cycles. The FIR and sensitivities showed excellent reversibility and stability ( < 4%) based on the FIR curves. The FIR curves in the cooling and heating of first cycle almost resembles the second cycle within the range of temperatures studies (30–300 °C) without any degradation or

**Table 3**
Temperature sensing characteristics of the **FIR** based on TCL and NTCL methods in different lanthanide doped materials.

| Composition | Temperature range (K) | Maximum Sensitivity | | Reference |
|---|---|---|---|---|
| | | $S_A$ ($K^{-1}$) | $S_R$ (% $K^{-1}$) | |
| **FIR based on TCL** | | | | |
| BLW:Er/Tm/Yb | 30–300 | 0.0012 @ 190 K | 42.7 @ 30 K | Present work |
| SLA:Er/Yb0.1 | 15–300 | 0.024 @ 300 K | 283 @ 15 K | [15] |
| $YbNbO_4:Er^{3+}$ | 100–280 | 0.0071 @ 220 K | – | [45] |
| $YOF:Pr^{3+}$ | 90–300 | 0.00567 @ 380 K | 9.4 @ 90 K | [46] |
| $LaF_3:Pr^{3+}$ ($C_{pr}$ = 20 %) | 80–320 | 0.017 @ 320 K | 3.1 @ 80 K | [47] |
| $Na_{0.5}Bi_{0.5}TiO_3$: $Ho^{3+}/Yb^{3+}$ | 167–377 | 0.009 @ 167 K | 6.14 @ 167 K | [48] |
| $CSMS:Eu^{2+}/Tb^{3+}$ | 77–280 | 0.047 @ 280 K | 0.6 @ 280 K | [49] |
| $TeO_2$–$PbCl_2$–$WO_3$: $Er^{3+}$ | 100–300 | 0.0005 @ 100 k | – | [50] |
| **FIR based on NTCL** | | | | |
| BLW:Er/Tm/Yb (NTCL) | 30–300 | 0.1737 @ 150 K | 0.7278 at 110 K | Present work |
| $Sr_3MoO_6:Eu^{3+}$/ $Tb^{3+}$ | 15–300 | 0.0029 @ 300 K | 0.262 @ 15 K | [51] |
| $CaF_2:Eu^{3+}/Tb^{3+}$ | 21–300 | – | 0.4 (constant) | [52] |
| $Gd_2(MoO_4)_3$: $Eu^{3+}$/ $Tb^{3+}$ | 80–450 | – | 0.52 @ 300 K | [53] |
| $LNO:Er^{3+}/Yb^{3+}$ | 14–300 | 0.172 @ 210 K | 548 @ 14 K | [54] |
| $YTiYb:Ho^{3+}$/ $30Zn^{2+}$ | 100–300 | 0.057 @ 300 | – | [55] |
| $YTiYb:Ho^{3+}$/ $20Zn^{2+}$ | 100–300 | 0.0046 @ 260 | – | [55] |
| $Y_2O_3:Er^{3+}/Yb^{3+}$ | 150–300 | – | 1.57 (constant) | [56] |

deviations. Thus, the material BLW:Er/Tm/Yb phosphor tends to exhibit constant sensitivity in the cryogenic temperature range with minimum deviation and good repeatability.

### 3.5. CIE coordinates at cryogenic temperatures

Fig. 8 shows the temperature dependent variation in CIE coordinates of the tri-doped BLW:Er/Tm/Yb in the range 30–300 K. A significant color change from greenish yellow to yellow with increase in temperature can be seen in the CIE graph. But the considerable resolution in xy values starting from 90 K. And the values calculated were relatively similar to that of Philips-hue- color values [57].

## 4. Conclusions

Aurivillius family perovskite bismuth lanthanum tungstate (BLW) doped with two activators ($Er^{3+}$ and $Tm^{3+}$) and a sensitizer ($Yb^{3+}$) that are well known for their upconversion efficiencies were prepared and characterized. The structural and morphological results indicate the formation of pure phase material without any impure phases. Upconversion (UC) spectra of the tri-doped BLW show five significant UC bands, two individually from two activator ions and one as a convoluted UC band with contribution from both $Er^{3+}$ and $Tm^{3+}$ ions. The temperature dependence of the integrated intensity of UC bands follow the modified Arrhenius equation and the ratios were thus theoretically fit accordingly. One thermally coupled (TCL) related FIR has been identified in $Er^{3+}$ UC related to $^2H_{11/2} \rightarrow {}^4I_{15/2}/{}^4S_{3/2} \rightarrow {}^4I_{15/2}$ which has been fit through Boltzmann's distribution law and all the other FIRs are non-thermally coupled (NTCL). Totally eight NTCL FIRs (one for each activator ion and six for the combination) have been fit using modified

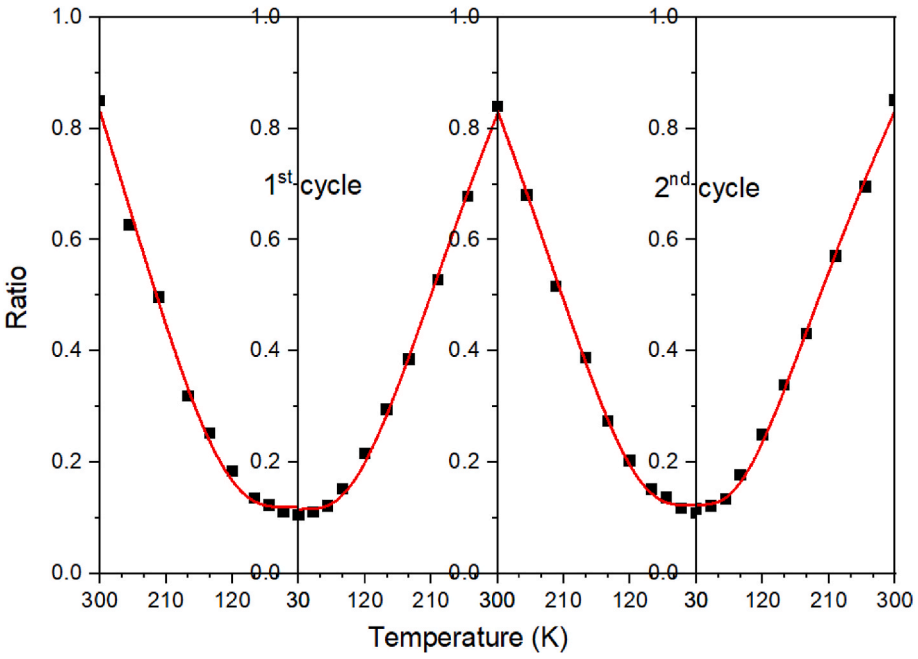


**Fig. 7.** Fluorescence intensity ratio for the integrated intensities of peaks at 525 nm/545 nm in BLW:Er/Tm/Yb phosphor materials as a function of temperature in repeated cycles in the temperature range 30–300 °C.

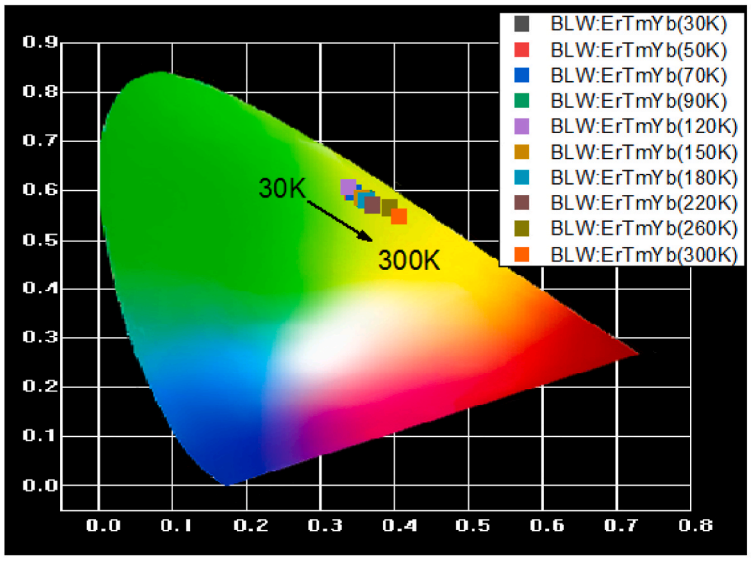


| Temperature (K) | x | y |
|---|---|---|
| 30 | 0.3586 | 0.5811 |
| 50 | 0.3391 | 0.5958 |
| 70 | 0.3413 | 0.5944 |
| 90 | 0.3559 | 0.583 |
| 120 | 0.3348 | 0.6055 |
| 150 | 0.352 | 0.5852 |
| 180 | 0.3587 | 0.5782 |
| 220 | 0.3674 | 0.5698 |
| 260 | 0.3893 | 0.5643 |
| 300 | 0.4032 | 0.5467 |

**Fig. 8.** CIE chromaticity diagram with color coordinates of BLW: ErTm/Yb as a function of temperature in the range 30–300 K (Table show the respective x,y values). (For interpretation of the references to color in this figure legend, the reader is referred to the Web version of this article.)

Arrhenius equation. In the present study it has been found that in the tri-doped BLW phosphor material, TCL based FIR of $Er^{3+}$ (0.43 % $K^{-1}$) achieved the highest relative sensitivity at 300 K compared to NTCL based FIR while energy transfer and quenching mechanisms among the activator ions making the NTCL based FIR less sensitive. Repeatability of the TCL based FIR was also checked and it showed minimum deviation from one cycle to that other proving the materials ability for practical purposes in cryogenic temperature range.

## Data and code availability

The authors are sole responsible for data and materials used. The data and the materials can be re-produced under specified conditions in the experimental section and available upon request.

## Ethical statement

The authors state that the work done in the manuscript does not contain any experiments involving human/animal tissue and according to the journal ethical policy, all the ethical guidelines were followed.

## Declaration of competing interest

The authors declare that they have no known competing financial interests or personal relationships that could have appeared to influence the work reported in this paper.

## Acknowledgments

This work is funded by national funds (OE), through FCT, Portugal, I. P., in the scope of the framework contract foreseen in the numbers 4, 5 and 6 of the article 23, of the Decree-Law 57/2016, of August 29, changed by Law 57/2017, of July 19 and also within the scope of the project i3N, UIDB/50025/2020 & UIDP/50025/2020, financed by national funds through the FCT/MEC.

## References

[1] M.-H. Fang, K.-C. Chen, N. Majewska, T. Leśniewski, S. Mahlik, G. Leniec, S. M. Kaczmarek, C.-W. Yang, K.-M. Lu, H.-S. Sheu, R.-S. Liu, Hidden structural evolution and bond valence control in near-infrared phosphors for light-emitting diodes, ACS Energy Lett. 6 (2021) 109–114, https://doi.org/10.1021/acsenergylett.0c02373.

[2] J. Xu, J. Ueda, S. Tanabe, Design of deep-red persistent phosphors of $Gd_3Al_5$-$xGa_xO_{12}$:$Cr^{3+}$ transparent ceramics sensitized by $Eu^{3+}$ as an electron trap using conduction band engineering, Opt. Mater. Express 5 (2015) 963–968, https://doi.org/10.1364/OME.5.000963.

[3] Q. Chen, J. Wu, X. Ou, B. Huang, J. Almutlaq, A.A. Zhumekenov, X. Guan, S. Han, L. Liang, Z. Yi, J. Li, X. Xie, Y. Wang, Y. Li, D. Fan, D.B.L. Teh, A.H. All, O. F. Mohammed, O.M. Bakr, T. Wu, M. Bettinelli, H. Yang, W. Huang, X. Liu, All-inorganic perovskite nanocrystal scintillators, Nature 561 (2018) 88–93, https://doi.org/10.1038/s41586-018-0451-1.

[4] L. Luo, W. Ran, P. Du, W. Li, D. Wang, Photocatalytic and thermometric characteristics of $Er^{3+}$-activated $Bi_5IO_7$ upconverting microparticles, Adv. Mater. Interfac. 7 (2020), 1902208, https://doi.org/10.1002/admi.201902208.

[5] M.D. Dramićanin, Trends in luminescence thermometry, J. Appl. Phys. 128 (2020), https://doi.org/10.1063/5.0014825.

[6] T.P. Jenkins, C.F. Hess, S.W. Allison, J.I. Eldridge, Measurements of turbine blade temperature in an operating aero engine using thermographic phosphors, Meas. Sci. Technol. 31 (2020), 44003, https://doi.org/10.1088/1361-6501/ab4c20.

[7] C. Zaldo, 10 - lanthanide-based luminescent thermosensors: from bulk to nanoscale, in: P. Martín-Ramos, M.B.T. Ramos Silva (Eds.), Adv. Nanomater., Elsevier, 2018, pp. 335–379, https://doi.org/10.1016/B978-0-12-813840-3.00010-7. -L.-B.M.M.

[8] M. Back, J. Ueda, J. Xu, D. Murata, M.G. Brik, S. Tanabe, Ratiometric luminescent thermometers with a customized phase-transition-driven fingerprint in perovskite oxides, ACS Appl. Mater. Interfaces 11 (2019) 38937–38945, https://doi.org/10.1021/acsami.9b13010.

[9] M. Maczka, W. Paraguassu, A.G.S. Filho, P.T.C. Freire, J.M. Filho, J. Hanuza, Phonon-instability-driven phase transitions in ferroelectric $Bi_2WO_6$:$Eu^{3+}$: high-pressure Raman and photoluminescence studies, Phys. Rev. B 77 (2008), 94137, https://doi.org/10.1103/PhysRevB.77.094137.

[10] P.P. Shanbogh, V.C. Petwal, J. Dwivedi, A. Rao, N.G. Sundaram, High-energy electron-beam-induced evolution of secondary phase and enhanced photocatalytic activity in monoclinic $BiEuWO_6$ nanoparticles, J. Phys. Chem. C 123 (2019) 10881–10892, https://doi.org/10.1021/acs.jpcc.8b12368.

[11] A. Khalid, K. Kontis, Thermographic phosphors for high temperature measurements: principles, current state of the art and recent applications, Sensors 8 (2008) 5673–5744, https://doi.org/10.3390/s8095673.

[12] S.A. Wade, S.F. Collins, G.W. Baxter, Fluorescence intensity ratio technique for optical fiber point temperature sensing, J. Appl. Phys. 94 (2003) 4743–4756, https://doi.org/10.1063/1.1606526.

[13] S. Chen, W. Song, J. Cao, F. Hu, H. Guo, Highly sensitive optical thermometer based on FIR technique of transparent $NaY_2F_7$:$Tm^{3+}$/$Yb^{3+}$ glass ceramic, J. Alloys Compd. 825 (2020), 154011, https://doi.org/10.1016/j.jallcom.2020.154011.

[14] K. Pavani, J. Suresh Kumar, K. Srikanth, M.J. Soares, E. Pereira, A.J. Neves, M.P. F. Graça, Highly efficient upconversion of $Er^{3+}$ in $Yb^{3+}$ codoped non-cytotoxic strontium lanthanum aluminate phosphor for low temperature sensors, Sci. Rep. 7 (2017) 1–15, https://doi.org/10.1038/s41598-017-17725-z.

[15] J.S. Kumar, K. Pavani, M.P.F. Graça, M.J. Soares, Sharp photoluminescence of $Pr^{3+}$ ions in yttrium oxyfluoride nanospheres : thermographic phosphor characteristics using the fluorescence intensity ratio technique, Mater. Lett. X. 6 (2020), 100041, https://doi.org/10.1016/j.mlblux.2020.100041.

[16] K. Pavani, J.P.C. do Nascimento, S.K. Jakka, F.F. do Carmo, A.J.M. Sales, M. J. Soares, M.P.F. Graça, F.J.A. de Aquino, D.X. Gouveia, A.S.B. Sombra, Analogy of different optical temperature sensing techniques in $LaNbO_4$:$Er^{3+}$/$Yb^{3+}$ phosphor, J. Lumin. 235 (2021) 117992, https://doi.org/10.1016/j.jlumin.2021.117992.

[17] Xue Liu, Sebastiaan Akerboom, Mathijs de Jong, Ilpo Mutikainen, Stefania Tanase, Andries Meijerink, Elisabeth Bouwman, Mixed-lanthanoid metal–organic framework for ratiometric cryogenic temperature sensing, Inorg. Chem. 54 (23) (2015) 11323–11329, https://doi.org/10.1021/acs.inorgchem.5b01924.

[18] Artur Tymiński, Inocencio R. Martín, Tomasz Grzyb, Upconversion in detail: multicolor emission of Yb/Er/Tm-doped nanoparticles under 800, 975, 1208,and 1532 nm excitation Wavelengths Part, Part. Syst. Charact. (2020) 2000068, https://doi.org/10.1002/ppsc.202000068.

[19] S. Liu, J. Cui, J. Jia, J. Fu, W. You, Q. Zeng, Y. Yang, X. Ye, High sensitive $Ln^{3+}$/$Tm^{3+}$/$Yb^{3+}$ ($Ln^{3+}$=$Ho^{3+}$,$Er^{3+}$) tri-doped $Ba_3Y_4O_9$ upconverting optical thermometric materials based on diverse thermal response from non-thermally coupled energy levels, Ceram. Int. 45 (2019) 1–10, https://doi.org/10.1016/j.ceramint.2018.09.162.

[20] K. Upendra Kumar, N. Vijaya, Jorge Oliva, C. Jacinto, E. De la Rosa, C. K. Jayasankar, Multicolor upconversion emission and color tunability in $Tm^{3+}$/$Er^{3+}$/$Yb^{3+}$ tri-doped $NaNbO_3$ nanocrystals, Materials Express 2 (4) (2012) 294–302, https://doi.org/10.1166/mex.2012.1088.

[21] Yannick Ledemi, Andrée-Anne Trudel, Victor A.G. Rivera, Sébastien Chenu, Emmanuel Véron, Luiz Antonio Nunes, Mathieu Allix, Younès Messaddeq, White light and multicolor emission tuning in triply doped Yb3+/Tm3+/Er3+ novel fluoro-phosphate transparent glass-ceramics, J. Mater. Chem. C 2 (2014) 5046–5056, https://doi.org/10.1039/C4TC00455H.

[22] H. Ait ahsaine, M. Ezahri, A. Benlhachemi, B. Bakiz, S. Villain, J.-C. Valmalette, F. Guinneton, M. Arab, J.-R. Gavarri, Structural, vibrational study and UV photoluminescence properties of the system $Bi_{(2-x)}Lu_{(x)}WO_6$ ($0.1 \leq x \leq 1$), RSC Adv. 5 (2015) 96242–96252, https://doi.org/10.1039/C5RA19424E.

[23] K. Pavani, M.P.F. Graça, J.S. Kumar, A.J. Neves, Photoluminescence varied by selective excitation in $BiGdWO_6$:$Eu^{3+}$ phosphor, Opt. Mater. 74 (2017) 120–127, https://doi.org/10.1016/j.optmat.2017.03.038.

[24] S. Salmaoui, F. Sediri, N. Gharbi, C. Perruchot, M. Jouini, Hexagonal hydrated tungsten oxide nanomaterials: hydrothermal synthesis and electrochemical properties, Electrochim. Acta 108 (2013) 634–643, https://doi.org/10.1016/j.electacta.2013.07.086.

[25] L. Liu, J. Jiang, S. Jin, Z. Xia, M. Tang, Hydrothermal synthesis of β-bismuth oxide nanowires from particles, CrystEngComm 13 (2011) 2529–2532, https://doi.org/10.1039/C0CE00773K.

[26] R. Parmar, R.S. Kundu, R. Punia, N. Kishore, P. Aghamkar, Fe2O3 modified physical, structural and optical properties of bismuth silicate glasses, J. Mater. (2013), 650207, https://doi.org/10.1155/2013/650207, 2013.

[27] N. Tian, Y. Zhang, H. Huang, Y. He, Y. Guo, Influences of Gd substitution on the crystal structure and visible-light-driven photocatalytic performance of $Bi_2WO_6$, J. Phys. Chem. C 118 (2014) 15640–15648, https://doi.org/10.1021/jp500645p.

[28] Wei Wei, Yan Zhang, Rui Chen, Julian Goggi, Na Ren, Ling Huang, K. Kishore, Bhakoo, handong sun, and timothy thatt yang tan, cross relaxation induced pure red upconversion in activator- and sensitizer-rich lanthanide nanoparticles, Chem. Mater. 26 (2014) 5183–5186, https://doi.org/10.1021/cm5022382.

[29] S. Hu, X. Wu, Z. Tang, Z. Xi, Z. Chen, P. Hu, Y. Yu, H. Yan, Y. Liu, Upconversion $NaYF_4$ nanoparticles for size dependent cell imaging and concentration dependent detection of rhodamine B, J. Nanomater. (2015), 598734, https://doi.org/10.1155/2015/598734, 2015.

[30] B. Zhou, Z. Xiao, A. Huang, L. Yan, F. Zhu, J. Wang, P. Yin, H. Wang, Effect of Tm–Er concentration ratio on the photoluminescence of Er–Tm:$Al_2O_3$ thin films fabricated by pulsed laser deposition, Prog. Nat. Sci. 18 (2008) 661–664, https://doi.org/10.1016/j.pnsc.2008.01.009.

[31] J. Méndez-Ramos1, V.D. Rodriguez1, V.K. Tikhomirov, J. del-Castillo, A.C. Yanes, $Yb^{3+}$-$Er^{3+}$-$Tm^{3+}$ co-doped nano-glass-ceramics tuneable up-conversion phosphor, Eur. Phys. J. Appl. Phys. 43 (2008) 149–153, https://doi.org/10.1051/epjap:2008101.

[32] Prasenjit prasad sukul, Amitabh, Kaushal Kumar, Near infrared to visible upconversion studies on $Er^{3+}$/$Yb^{3+}$/$Tm^{3+}$ doped $PbZrTiO_3$ multifunctional ceramics, OSA Continuum 3 (2018) 1089, https://doi.org/10.1364/OSAC.1.001087.

[33] Marcin Runowski, Przemysław Woźny, Natalia Stopikowska, Inocencio R. Martín, Víctor Lavín, Stefan Lis, Luminescent nanothermometer operating at very high temperature sensing up to 1000 K with upconverting nanoparticles ($Yb^{3+}$/$Tm^{3+}$), ACS Appl. Mater. Interfaces 12 (2020) 43933–43941, https://doi.org/10.1021/acsami.0c13011.

[34] E.H. Song, S. Ding, M. Wu, S. Ye, Z.T. Chen, Y.Y. Ma, Q.Y. Zhang*, Tunable white upconversion luminescence from $Yb^{3+}$-$Tm^{3+}$-$Mn^{2+}$ tri-doped perovskite Nanocrystals, Opt. Mater. Express 4 (2014) 1186, https://doi.org/10.1364/OME.4.001186.

[35] H. Liu, M. Liu, K. Wang, B. Wang, X. Jian, G. Bai, Y. Zhang, Efficient upconversion emission and high-sensitivity thermometry of $BaIn_2O_4$:$Yb^{3+}$/$Tm^{3+}$/$RE^{3+}$ (RE = $Er^{3+}$, $Ho^{3+}$) phosphor, Dalton Trans. 50 (2021) 12107–12117, https://doi.org/10.1039/D1DT01854J.

[36] C.D.S. Brites, A. Millán, L.D. Carlos, Chapter 281 - lanthanides in luminescent thermometry, in: B. Jean-Claude, P.B.T.-H. on the P, C. of, R.E. Vitalij K (Eds.), Incl. Actinides, Elsevier, 2016, pp. 339–427, https://doi.org/10.1016/bs.hpcre.2016.03.005.

[37] Y. Fang, L. Wang, Q. Sun, T. Lu, Z. Deng, Z. Ma, Y. Jiang, H. Jia, W. Wang, J. Zhou, H. Chen, Investigation of temperature-dependent photoluminescence in multi-quantum wells, Sci. Rep. 5 (2015), 12718, https://doi.org/10.1038/srep12718.

[38] M. Quintanilla, E. Cantelar, F. Cussó, M. Villegas, A.C. Caballero, Temperature sensing with up-converting submicron-sized LiNbO3:$Er^{3+}$/$Yb^{3+}$Particles, Appl. Phys. Express. 4 (2011), 22601, https://doi.org/10.1143/apex.4.022601.

[39] V.K. Rai, Temperature sensors and optical sensors, Appl. Phys. B 88 (2007) 297–303, https://doi.org/10.1007/s00340-007-2717-4.

[40] S.F. León-Luis, U.R. Rodríguez-Mendoza, E. Lalla, V. Lavín, Temperature sensor based on the $Er^{3+}$ green upconverted emission in a fluorotellurite glass, Sens. Actuators B. Chem. 158 (2011) 208–213, https://doi.org/10.1016/j.snb.2011.06.005.

[41] A. Pandey, V.K. Rai, Optical thermometry using FIR of two close lying levels of different ions in $Y_2O_3$:$Ho^{3+}$–$Tm^{3+}$–$Yb^{3+}$ phosphor, Appl. Phys. B 113 (2013) 221–225, https://doi.org/10.1007/s00340-013-5460-z.

[42] Teng Zheng, Marcin Runowski, Natalia Stopikowska, Małgorzata Skwierczyńska, Stefan Lis, Du Peng, Laihui Luo, Dual-center thermochromic $Bi_2MoO_6$:$Yb^{3+}$, $Er^{3+}$, $Tm^{3+}$ phosphors for ultrasensitive luminescence thermometry, J. Alloys Compd. 890 (2021), 161830, https://doi.org/10.1016/j.jallcom.2021.161830.

[43] Carlos Alarcón-Fernández, Carlos Zaldo, Concepción Cascales, Er3+ Yb, $Tm^{3+}$ co-doped β'$Gd_2(MoO_4)_3$ for high sensitivity luminescence thermometry spanning from 300 to 890 K, J. Alloys Compd. 913 (2022), 165180, https://doi.org/10.1016/j.jallcom.2022.165180.

[44] Yan Zhao, Rui Hu, Xusheng Wang, Yanxia Li, Low temperature reliability and high sensitivity of dual-channel up-conversion thermometry phosphor optimized by heterovalent ions, Mater. Res. Bull. 139 (2021), 111264, https://doi.org/10.1016/j.materresbull.2021.111264.

[45] Heming Ji, Xunze Tang, Haiyan Zhang, Xiaolong Li, Yannan Qian, Optical temperature sensing of $YbNbO_4:Er^{3+}$ phosphors synthesized by hydrothermal method, Coatings 11 (2021) 383, https://doi.org/10.3390/coatings11040383.

[46] J. Suresh Kumar, K. Pavani, M.P.F. Graça, M.J. Soares, Sharp photoluminescence of Pr3+ ions in yttrium oxyfluoride nanospheres: thermographic phosphor characteristics using the fluorescence intensity ratio technique, Mater. Lett. X 6 (2020) 100041, https://doi.org/10.1016/j.mlblux.2020.100041.

[47] Maksim S. Pudovkin, Oleg A. Morozov, Vitaly V. Pavlov, Stella L. Korableva, Elena V. Lukinova, Yury N. Osin, Vladimir G. Evtugyn, Roman A. Safiullin, Vadim V. Semashko, J. Nanomater. 2017 (2017), https://doi.org/10.1155/2017/3108586. Article ID 3108586.

[48] Yuzhen Wang, Yanan Wang, Chaoyang Ma, Zhe Feng, Chuandong Zuo, Wanggui Ye, Chong Zhao, Yanbin Li, Zicheng Wen, Zhiquan Cao, Zhijun Cao, Xiaofei Shen, Chong Wang, Yingkui Li, Xuanyi Yuan, Yongge Cao, Excellent cryogenic optical thermometry based on green up-conversion of Ho3+-doped perovskite Na0.5Bi0.5TiO3 ceramics, J. Mater. Chem. C 9 (2021) 1353–1361, https://doi.org/10.1039/D0TC04906A.

[49] Ke Su, Qingfeng Guo, Pengfei Shuai, Ning Liu, Lefu Mei, Libing Liao, A novel Eu2+/Tb3+ co-doped phosphor with pyroxene structure applied for cryogenic thermometric sensing, J. Am. Ceram. Soc. (2021), https://doi.org/10.1111/jace.18275 first published.

[50] R. Yatskiv, P. Kostka, J. Grym, J. Zavadil, Temperature sensing down to 4 K with erbium-doped tellurite glasses, J. Non-Cryst. Solids 575 (2022) 121183, https://doi.org/10.1016/j.jnoncrysol.2021.121183.

[51] D.V.M. Paiva, S.K. Jakka, M.A.S. Silva, J.P.C. do Nascimento, M.P.F. Graça, A.S. B. Sombra, M.J. Soares, S.E. Mazzetto, P.B.A. Fechine, K. Pavani, Investigation on luminescence based optical temperature sensing behavior of Sr3MoO6:Eu3+/Tb3+, Optik 246 (2021) 167825, https://doi.org/10.1016/j.ijleo.2021.167825.

[52] Fangfang Hu, Zhangmei Zhao, Fengfeng Chi, Xiantao Wei, Min Yin, Structural characterization and temperature-dependent luminescence of CaF2:Tb3+/Eu3+ glass ceramics, J. Rare Earths 35 (2017) 536–541, https://doi.org/10.1016/S1002-0721(17)60945-1.

[53] Le Han, Jiaqiang Liu, Peng Liu, Bohan Li, Xianliang Li, Yan Xu, Dual-emissive Eu3+, Tb3+ co-doped Gd2(MoO4)3 phosphor for optical thermometry application, J. Phys. Chem. Solid. 153 (2021) 110032, https://doi.org/10.1016/j.jpcs.2021.110032.

[54] K. Pavani, J.P.C. do Nascimento, S.K. Jakka, F.F. do Carmo, A.J.M. Sales, M. J. Soares, M.P.F. Graça, F.J.A. de Aquino, D.X. Gouveia, A.S.B. Sombra, Analogy of different optical temperature sensing techniques in LaNbO4:Er3+/Yb3+ phosphor, J. Lumin. 235 (2021) 117992, https://doi.org/10.1016/j.jlumin.2021.117992.

[55] P.K. Vishwakarma, P.K. Shahi, S.B. Rai, A. Bahadur, Low temperature optical sensor based on non-thermally coupled level of Ho3+ and defect level of Zn2+ in Yb3+:Y2Ti2O7 phosphor, J. Phys. Chem. Solid. 142 (2020) 109445, https://doi.org/10.1016/j.jpcs.2020.109445.

[56] V. Lojpur, G. Nikolić, M.D. Dramićanina, Luminescence thermometry below room temperature via up-conversion emission of $Y2O3:Yb^{3+},Er^{3+}$ nanophosphors, J. Appl. Phys. 115 (2014), 203106, https://doi.org/10.1063/1.4880158.

[57] https://www.enigmaticdevices.com/philips-hue-lights-popular-xy-color-values/.